Development and Application of a Rod and Spherical-Shaped Viral Nanoparticle MRI Contrast Agent for Atherosclerosis Diagnosis

Michael A. Bruckman[1] and Nicole F. Steinmetz[1,2,3]*

Department of [1]Biomedical Engineering, [2]Radiology, [3]Materials Science and Engineering, Case Western Reserve University School of Medicine, 10900 Euclid Avenue, Cleveland, OH 44106, USA
*corresponding author: nicole.steinmetz@case.edu

ABSTRACT

Magnetic resonance imaging (MRI) has recently flourished as an impressive anatomical imaging modality for diagnosing internal injury, cancer, and cardiovascular diseases. Nanoparticle MRI contrast agents vastly improve imaging sensitivity for identifying and diagnosing diseases in soft tissue. A common challenge is the fabrication of nanoparticles with well-defined properties, such as morphology, size, charge, and surface functionalities. *Tobacco mosaic virus* (TMV) presents a hollow rod-shaped platform capable of undergoing chemical conjugation to its interior and exterior surfaces. Recently, it was found that TMV undergoes thermal transition to form RNA-free spherical nanoparticles (SNPs) upon heating for a short time period. Here, we show that TMV can be loaded with up to 3,500 paramagnetic gadolinium (Gd) ions to enhance MR sensitivity. Upon conjugation of chelated Gd compounds, the ionic relaxivity is significantly enhanced. Through thermal transition 170 nm-sized SNPs containing 25,000 Gd ions were formed; such SNPs reach T_1 relaxivities of over 400,000 $mM^{-1}s^{-1}$ per nanoparticle. TMV rods can undergo further chemical modification for targeted delivery of cargo. Here, we target the rods towards VCAM-1 receptors on activated endothelial cells *in vitro* as a model for atherosclerotic plaque targeting.

Keywords: Atherosclerosis, tobacco mosaic virus, MRI, VCAM-1, viral nanoparticles

1 INTRODUCTION

Coronary artery disease is among the leading causes of death around the world. The underlying cause of most deadly cardiac events, such as stroke and heart attacks, is inflammation in the form of atherosclerosis. Early diagnosis and treatment of atherosclerotic plaques will lead to better patient outcomes.

During the development of atherosclerosis, endothelial cells lining the intima overexpress a wide variety of cell adhesion molecules, selectins, and integrins [1]. Their extracellular display has been utilized to direct nanoparticles of various compositions to these sites for imaging and therapy [2]. In particular, vascular cell adhesion molecule (VCAM-1) receptors can be targeted throughout the progression of plaque development [3-5]. The significant overexpression of this adhesion molecule at atherosclerotic plaques has led to the development of many VCAM-1 targeted nanoparticle platforms [5,6]. Phage display technology has identified and produced an oligopeptide sequences specific for VCAM-1 receptors [7], thus opening the door for the development of tissue-specific contrast agents.

Magnetic resonance imaging (MRI) provides an optimal platform for imaging atherosclerotic plaques because of its high spatial resolution, soft tissue contrast and general safety. Unfortunately, early disease detection with MRI is difficult because diseased areas often have similar signal intensity compared to the surrounding healthy tissue. Therefore, signal enhancement using contrast agents is required. Contrast agents interact with water molecules in the body to affect the T_1 or T_2 proton relaxation which give rise to positive or negative signal change, respectively [8]. Chelated paramagnetic lanthanide ions, such as gadolinium, are the most common T_1 relaxivity contrast agents [9]. Small molecule complexes of Gd are currently used in the clinic, but their sensitivity for disease detection is low. The use of nanoparticles to enhance MRI sensitivity towards contrast agents has shown great potential in imaging and diagnosing diseases such as cancer and cardiovascular disease [10].

Nanotechnology has revolutionized the MRI field. Nanoparticles, a particle with one or more dimensions of 100 nm or less, can be loaded with high payloads of multiple cargos, e.g. image contrast agents, therapeutics, and/or targeting ligands for direction to sites of disease [11]. The targeted delivery of nanoparticles carrying image contrast agents and therapeutics leads to earlier and more accurate diagnosis and more efficacious therapy. Nanoparticles have been engineered for MRI contrast by based on gold [12], silicon [13], carbon nanotubes [14] and fullerenes [15], polymers and dendrimers [16], liposomes and micelles [17], and viral nanoparticles [18,19]. Binding chelated paramagnetic ions to nanoparticle platforms enhances the MRI sensitivity in two ways; first, the ionic relaxivity (brightness per ion) increases due to reduced molecular rotation times (τ_R), and second, nanoparticles deliver a high concentration of chelated ions to the site of disease [20].

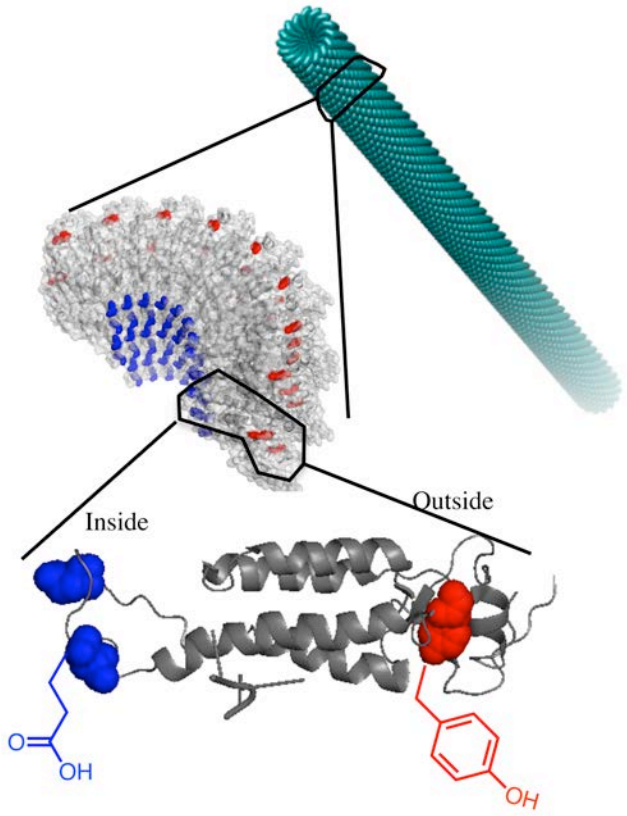

Figure 1 A crystal structure representation (PyMol and Chimera UCSD) of tobacco mosaic virus highlighting the interior glutamic acids, GLU97 and GLU106 (blue), and exterior tyrosine, TYR139 (red), for bioconjugation.

A common challenge in engineering nanoparticle MRI contrast agents is fabrication with well-defined properties, such as shape, size, charge, and surface properties. Viral nanoparticles (VNPs) provide an excellent platform for biomedical applications because they are highly monodisperse, capable of undergoing chemical and genetic modification, easily attainable, and available in a variety of sizes and morphologies [21]. Only spherical shaped viral nanoparticles have been utilized as potential MRI contrast agents, including cowpea mosaic virus [22], cowpea chlorotic mottle virus [23], bacteriophage MS2 [24], bacteriophage Qβ [25], and bacteriophage P22 [19].

Tobacco mosaic virus (TMV) presents a robust, rod-shaped platform measuring 300 by 18 nm with a 4 nm hollow channel, capable of undergoing chemical conjugation to its interior and exterior surfaces (Figure 1) [26]. This stiff rod-shaped nanoparticle has been utilized for a variety of applications in nanotechnology [27,28]. Chemically and genetically engineered TMV particles are being developed and tested for applications as light harvesting systems [29,30], energy storage [31], sensing [32], and cell growth [26,33]. Recently, it was found that TMV undergoes thermal transition to form RNA-free spherical nanoparticles (SNPs) upon heating for a short time period (Figure 3) [34]. The size of the SNPs can be controlled to be 50 to 500 nm by tuning the TMV concentration.

Here we show that TMV can be loaded with a very high number of paramagnetic Gd ions to enhance MRI sensitivity. Both the exterior and interior surfaces of TMV were successfully labeled with Gd(DOTA) molecules by targeting tyrosine residues and glutamic acid residues, respectively. The interior modified particles were able to undergo thermal transition to form stable RNA-free spherical nanoparticles with very high Gd loading per nanoparticle [18]. Finally, VCAM-1 peptide labeled TMV particles specifically targeted activated endothelial cells *in vitro*.

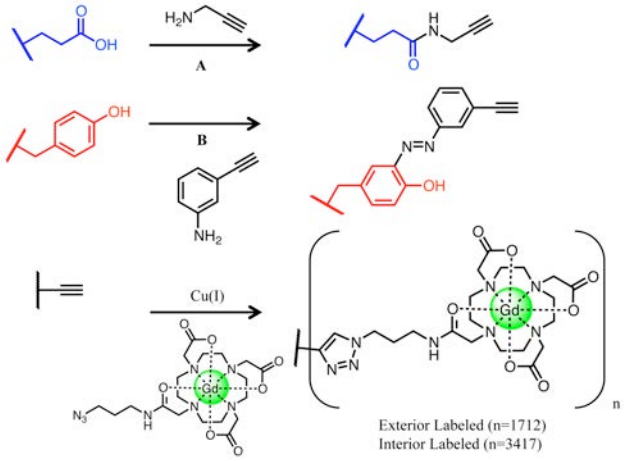

Figure 2 Schematic illustration of bioconjugation reactions used to incorporate terminal alkynes to the interior and exterior of TMV. CuAAC reaction of terminal alkyne labeled TMV with Gd-DOTA azide.

2 RESULTS/DISCUSSION

Tobacco mosaic virus (TMV) was extracted from *Nicotiana benthamiana* plants yielding 4.5 mg virus per gram of infected leaf material [35]. Using this one-day purification protocol of just over 100 g leaf material, we obtained over 500 mg of TMV. The purified TMV particles were then subject to established interior or exterior bioconjugation techniques incorporating terminal alkyne residues (Figure 1) [26,36]. The well-defined crystal structure of TMV (Figure 1) allows us to "see" where the interior and exterior reactive amino acids are located throughout the hollow rod-shaped TMV. Highlighted in red are the tyrosine residues (TYR139) on the exterior surface that are reactive toward diazonium salts. Highlighted in blue are the glutamic acid residues (GLU97 and GLU106), which are susceptible to EDC coupling with a primary amine. As shown in Figure 2, the bioconjugation of these amino acids provides a terminal alkyne handle for subsequent copper-catalyzed azide-alkyne cycloaddition (CuAAC) with azide groups. In order to create an MRI contrast agent, we chelated Gd ions to an azido labeled DOTA molecule (1,4,7,10-tetraazacyclododecane-1,4,7,10-tetraacetic acid) which was then conjugated to the terminal

alkyne labeled TMV particles. Following sucrose gradient purification, interior Gd labeled TMV (iGd-TMV) and exterior Gd labeled TMV (eGd-TMV) structural integrity was confirmed with transmission electron microscopy (TEM) and size exclusion chromatography (SEC) (Figure 3 B-E). The labeling efficiency was confirmed with matrix-assisted laser desorption/ionization time-of-flight mass spectrometry (MALDI-TOF MS) and inductively coupled plasma optical emission spectroscopy (ICP-OES). ICP-OES indicated that the eGd-TMV and iGd-TMV contained over 1700 and 3400 Gd per TMV particle. Spherical nanoparticle (SNPs) derivatives of the rod-shaped TMV were made by heating a 0.1 mg/ml solution of iGd-TMV for 15 s at 96°C (Figure 4). TEM and dynamic light scattering (DLS) indicated that the SNPs measured 170 nm in diameter and ICP-OES measured over 25,000 Gd per SNP.

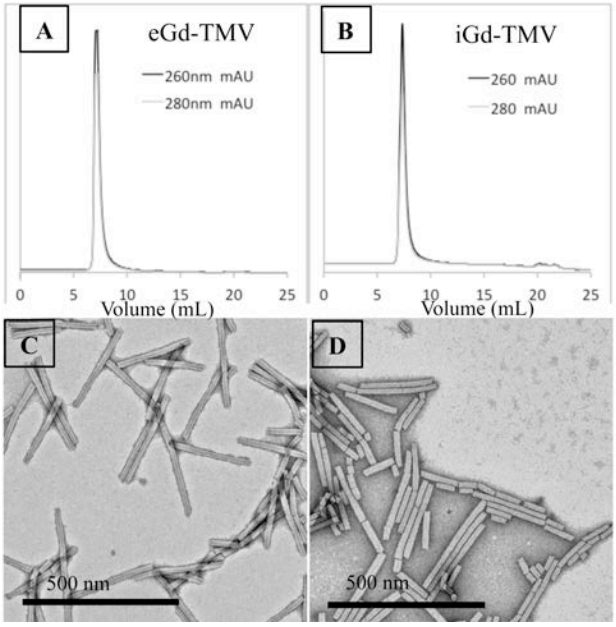

Figure 3 Size exclusion chromatograms of (A) eGd-TMV and (B) iGd-TMV. TEM image of (C) eGd-TMV and (D) iGd-TMV.

The ionic relaxivity of the Gd-loaded VNPs was tested on a clinical MRI (1.5T Siemens Espree). Using a standard inversion recovery sequence we determined the T_1 values, which were plotted against the concentration to yield the relaxivity in $mM^{-1}s^{-1}$. The measured ionic relaxivity values for eGd-TMV, iGd-TMV, and Gd-SNP was 15.7, 11.0, and 13.2 $mM^{-1}s^{-1}$ at 1.5T, which is two-three times higher than most commercially available contrast agents (between 4 and 5 $mM^{-1}s^{-1}$). The increased ionic relaxivity is due to reduced molecular rotational correlation time upon conjugation to the nanoparticle platform. Furthermore, we obtained per particle relaxivities for eGd-TMV, iGd-TMV, and Gd-SNP of 26,869, 37,519, and 340,758 $mM^{-1}s^{-1}$. These values represent the highest payload delivery for viral nanoparticle MRI contrast agents [18].

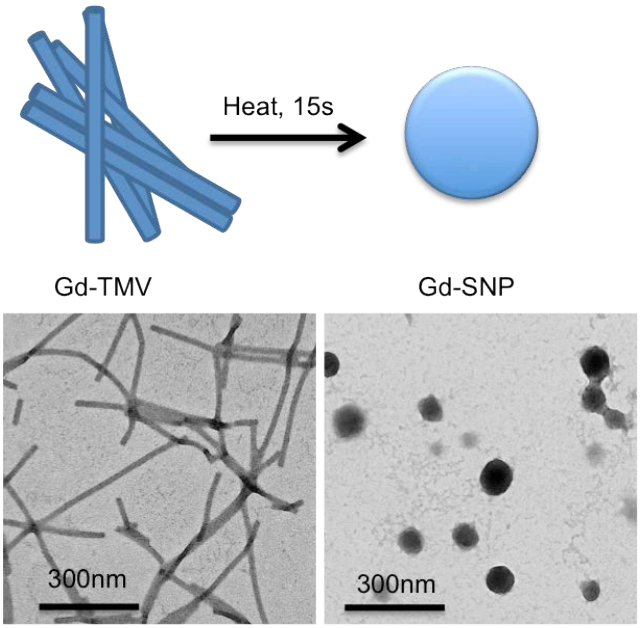

Figure 4 (Top) Thermal transition of TMV rods to spherical particles. (Bottom) TEM images of rod and spherical shaped particles.

In order to test the potential for *in vivo* targeting, we first utilized an *in vitro* cell model (SVEC4-10) of activated endothelial cells that overexpress VCAM-1 receptors. To test the targeting, two new TMV rod-based particles were synthesized: the targeted formulation used here was labeled with an azido derivative of the VCAM-1 peptide and fluorescein dyes for imaging (eVCAM-TMV). The second, non-targeted, formulation was labeled only with fluorescein dyes (native-TMV). Cell binding was characterized with flow cytometry. The flow cytometry results indicate a significant increase in activated cell binding for eVCAM-TMV particles (intensity = 734) over Native-TMV particles (intensity = 475) (Figure 5). Future experiments will combine the active targeting of VCAM-TMV and the MRI contrast enhancement of Gd labeled TMV particles to image atherosclerotic plaques in an atherosclerosis mouse model.

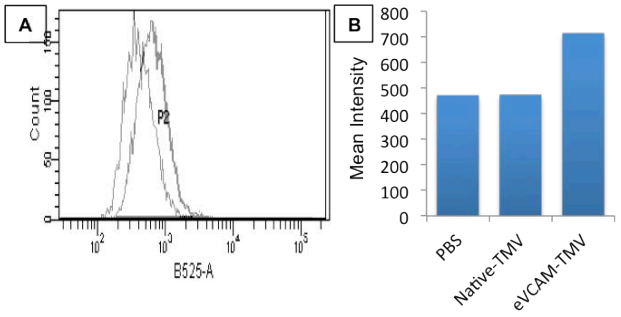

Figure 5 (A) Flow cytometry showing eVCAM-TMV and Native-TMV binding to activated endothelial cells. (B) A graph of the average fluorescence intensity representing the flow cytometry data.

3 CONCLUSION

Gd-loaded rod- and spherical-shaped viral nanoparticles demonstrated significant ionic relaxivity enhancement compared to free Gd(DOTA). The engineered particles have high potential for *in vivo* MRI contrast agent detection because of the high Gd loading per particle. These results represent the most sensitive viral nanoparticle MRI contrast agent to date. Aside from using carbon nanotubes, TMV-based MRI contrast agents have the highest aspect ratio for rod-shaped nanoparticles, of which there are very few options. This work lays the foundation for future biomedical applications. For example, conjugation of a targeting ligand, e.g. VCAM-1 peptide, directs the rod-shaped particles towards activated endothelial cells and thus provides an attractive platform for targeting the intima of atherosclerotic plaques.

4 ACKNOWLEDGEMENTS

This work was supported by NIH/NIBIB grant P30 EB011317, Mt. Sinai Foundation, and NIH T32 training grant (T32 HL105338-03).

5 REFERENCES

[1] Libby, P., DiCarli, M. & Weissleder, R. Journal of Nuclear Medicine 51, 33s-37s, 2010.
[2] Tardif, J.-C., Lesage, F., Harel, F. *et al.* Circulation Cardiovascular Imaging 4, 319-333, 2011.
[3] Yu, S. S., Ortega, R. A., Reagan, B. W. *et al.* Wiley Interdisciplinary Reviews: Nanomedicine and Nanobiotechnology 3, 620-646, 2011.
[4] Libby, P., Ridker, P. M. & Hansson, G. K. Nature 473, 317-325, 2011.
[5] Kelly, K. A., Allport, J. R., Tsourkas, A. *et al.* Circulation Research 96, 327-336, 2005.
[6] Deosarkar, S. P., Malgor, R., Fu, J. *et al.* Biotechnology and Bioengineering 101, 400-407, 2008.
[7] Nahrendorf, M., Jaffer, F. A., Kelly, K. A. *et al.* Circulation 114, 1504-1511, 2006.
[8] Caravan, P., Farrar, C. T., Frullano, L. *et al.* Contrast Media Mol. I. 4, 89-100, 2009.
[9] L Villaraza, A. J., Bumb, A. & Brechbiel, M. W. Chem. Rev. 110, 2921-2959, 2010.
[10] Zhou, Z. & Lu, Z. R. Wiley. Interdiscip. Rev. Nanomed. Nanobiotechnol. 5, 1-18, 2013.
[11] Parveen, S., Misra, R. & Sahoo, S. K. Nanomedicine: Nanotechnology, Biology, and Medicine 8, 147-166, 2012.
[12] Warsi, M. F. & Chechik, V. Phys. Chem. Chem. Phys. 13, 9812, 2011.
[13] Davis, J. J., Huang, W.-Y. & Davies, G.-L. J. Mater. Chem. 22, 22848-22850, 2012.
[14] Sitharaman, B., Kissell, K. R., Hartman, K. B. *et al.* Chem. Commun., 3915, 2005.
[15] Shu, C., Corwin, F. D., Zhang, J. *et al.* Bioconjugate Chem. 20, 1186-1193, 2009.
[16] Ye, M., Qian, Y., Shen, Y. *et al.* J. Mater. Chem. 22, 14369, 2012.
[17] Accardo, A., Tesauro, D., Aloj, L. *et al.* Coordin. Chem. Rev. 253, 2193-2213, 2009.
[18] Bruckman, M. A., Hern, S., Jiang, K. *et al.* J. Mater. Chem. B 1, 1482-1490, 2013.
[19] Qazi, S., Liepold, L. O., Abedin, M. J. *et al.* Mol. Parmaceutics, 120716120952001, 2012.
[20] Caravan, P. Chem. Soc. Rev. 35, 512-523, 2006.
[21] Yildiz, I., Shukla, S. & Steinmetz, N. F. Curr. Opin. Biotech. 22, 901-908, 2011.
[22] Prasuhn, D. E., Yeh, R. M., Obenaus, A. *et al.* Chem. Commun., 1269-1271, 2007.
[23] Allen, M., Bulte, J. W., Liepold, L. *et al.* Magn. Reson. Med. 54, 807-812, 2005.
[24] Garimella, P. D., Datta, A., Romanini, D. W. *et al.* J. Am. Chem. Soc. 133, 14704-14709, 2011.
[25] Pokorski, J. K., Breitenkamp, K., Liepold, L. O. *et al.* J. Am. Chem. Soc. 133, 9242-9245, 2011.
[26] Bruckman, M. A., Kaur, G., Lee, L. A. *et al.* ChemBioChem 9, 519-523, 2008.
[27] Soto, C. M. & Ratna, B. R. Curr. Opin. Biotech. 21, 426-438, 2010.
[28] Liu, Z., Qiao, J., Niu, Z. *et al.* Chem. Soc. Rev. 41, 6178-6194, 2012.
[29] Miller, R. A., Presley, A. D. & Francis, M. B. J. Am. Chem. Soc. 129, 3104-3109, 2007.
[30] Miller, R. A., Stephanopoulos, N., McFarland, J. M. *et al.* J. Am. Chem. Soc. 132, 6068-6074, 2010.
[31] Chen, X., Gerasopoulos, K., Guo, J. *et al.* ACS Nano 4, 5366-5372, 2010.
[32] Bruckman, M. A., Liu, J., Koley, G. *et al.* J. Mater. Chem. 20, 5715, 2010.
[33] Kaur, G., Valarmathi, M. T., Potts, J. D. *et al.* Biomaterials 31, 1732-1741, 2010.
[34] Atabekov, J., Nikitin, N., Arkhipenko, M. *et al.* J. Gen. Virol. 92, 453-456, 2011.
[35] Niu, Z., Bruckman, M. A., Li, S. *et al.* Langmuir 23, 6719-6724, 2007.
[36] Wu, L. Y., Zang, J. F., Lee, L. A. *et al.* J. Mater. Chem. 21, 8550-8557, 2011.